J Mater Sci (2007) 42:3675–3684
DOI 10.1007/s10853-006-1352-5

The tensile and creep behavior of Mg–Zn Alloys with and without Y and Zr as ternary elements

C. J. Boehlert

Received: 28 July 2005 / Accepted: 28 February 2006 / Published online: 30 January 2007

Abstract Tensile–creep experiments were conducted in the temperature range 100–200 °C and stress range 20–83 MPa for a series of magnesium–zinc–yttrium (Mg-Zn-Y) and mangnesium-zinc–zirconium (Mg-Zn-Zr) alloys ranging from 0 to 5.4 wt% Zn, 0 to 3 wt% Y, and 0 to 0.6 wt.% Zr. The greatest tensile–creep resistance was exhibited by an Mg–4.1Zn–0.2Y alloy. The room-temperature yield strength increased with increasing Y content for Mg–1.6–2.0Zn alloys. The greatest tensile strength and elongation was exhibited by Mg–5.4Zn–0.6Zr. This alloy also exhibited the finest grain size and the poorest creep resistance. The measured creep exponents and activation energies suggested that the creep mechanisms were dependent on stress. For applied stresses greater than 40 MPa, the creep exponents were between 4 and 8. For applied stresses less than 40 MPa, the creep exponent was 2.2. The calculated activation energies (Qapp) were dependent on temperature where the Q_{app} values between 100 and 150 °C (65 kJ/mol) were half those between 150 and 200 °C for the same applied stress value (30 MPa). Deformation observations indicated that the grain boundaries were susceptible to cracking in both tension and tension-creep, where at low applied stresses grain boundary sliding was suggested where strain accommodation occurred through grain boundary cracking. Thus grain size and grain boundaries appeared to be important microstructural parameters affecting the mechanical behavior. Microstructural effects on the tensile properties and creep behavior are discussed in comparison to other Mg-based alloy systems.

C. J. Boehlert (✉)
Chemical Engineering and Materials Science,
Michigan State University, 2527 Engineering Buidling, East Lansing, MI 48824, USA
e-mail: boehlert@egr.msu.edu

Introduction

In order to improve the creep strength of magnesium (Mg) alloys, rare earth and/or alkaline earth elements in small quantities have been effectively used as alloy additions [1–14]. For example, the creep rate of Mg–8wt.%Y[1] has been observed to be four orders of magnitude lower than AZ91 at 277 °C in the stress range 40–100 MPa [13]. This has been attributed to precipitation hardening, as precipitates can form in such high yttrium (Y) content Mg alloys. Precipitates in the Mg–8Y alloy can form both at grain boundaries as well as on dislocations through dynamic precipitation during creep at 277 °C [13]. Even small additions of Y have resulted in remarkably improved creep strength, where Y is a more potent creep strengthener than aluminum (Al) or manganese (Mn) [14]. Small additions of Zn have also proven to aid tensile and creep strength, especially when combined with a rare earth or alkaline earth element such as Y [13–18]. Finely dispersed metastable Y precipitates contribute significantly to the creep strength of Mg–Y alloys [19], while a RT yield stress of 610 MPa can be achieved in rapidly solidified powder metallurgy Mg–2.5Zn–6.8Y (Mg–1Zn–2Y(mol%)) containing nanometer-size

[1] All alloy compositions are given in weight percent unless otherwise mentioned.

grains [20–25]. However, such alloying elements are expensive and dense and in the case of Y, the metastable precipitates that form are unstable at elevated temperature and grow fast or transform to equilibrium precipitates which have negative effects on strengthening [19]. A high Y content is required to obtain a high density of metastable precipitates, and thus from a weight savings point of view, it would be beneficial to develop Mg alloys for structural applications, where creep strength is important, with lower Y contents.

Zinc concentrations as low as 0.05 wt% can provide a significant strengthening effect in Mg–Y alloys [13, 14, 16, 18]. In particular Suzuki et al. [13–15, 17] investigated the 650 K (377 °C) compressive creep strength (20–50 MPa) and found that a small concentration of Zn decreased the creep rate significantly, i.e. the minimum creep rate of Mg–3.1Y–0.06Zn and Mg–3.0Y–0.1Zn decreased by one order of magnitude compared to Mg–4Y. The same order of magnitude reduction in creep rate was observed at 550 K in Mg–1Y, but the strengthening by impurity Zn disappeared in a more Y-concentrated alloy, Mg–5.6Y, at this temperature [13, 17]. Therefore Zn is a potential candidate for reducing Y content without sacrificing useful elevated-temperature creep strength of Mg–Y alloys. The strengthening mechanism of Zn in Mg–Y alloys has not been fully understood as of yet and in particular the optimal concentration of Zn has yet to be discovered. This work evaluated the room-temperature (RT) and intermediate-temperature tensile and tensile creep behavior of Mg alloys with Zn concentrations between 0 and 5.4wt.% and Y concentrations between 0 and 3.0 wt%. In particular, the mechanical properties were evaluated at temperatures and stresses targeted for automotive applications, which are lower than those evaluated by Suzuki et al. [13–18]. In addition, the effect of 0–0.6wt.%Zr as a ternary element was evaluated for an alloy of composition similar to ZK60 and ZK61 [26, 27].

Experimental

The chemical composition of each alloy, given in Table 1, was determined using inductively coupled plasma and mass spectroscopy techniques. The blended elemental powders were hot pressed at 28 MPa for 1–2 h at 535 °C into a block using a 75 × 75 × 25 mm die. Metallographic samples were sectioned then mounted and polished using diamond paste, diamond thinner, and ethanol. Final polishing included 1 μm diamond paste for 30 min. Microstructural analysis was performed using a Quanta 200 Field Emission Gun Environmental Scanning Electron Microscope (ESEM) equipped with an energy dispersive spectroscopy (EDS) detector for elemental analysis. Grain size (d) was determined using the mean line-intercept method according to ASTM standard E112 [28], where over 50 grains were measured per sample and the average grain size was calculated. Fracture surfaces were examined in SEM using failed samples from both the tensile and tensile-creep testing.

Table 1 Compositions and grain sizes of the studied alloys

Alloy	Wt.%Zn	Wt.% Y	Wt.% Zr	Grain size, μm
Mg	0.017		0.003	242.6
Mg–2.9Zn	2.93		<0.001	106.5
Mg–3.3Zn	3.30		<0.001	155.6
Mg–4.0Zn	3.98		0.052	70.2
Mg–4.1Zn–0.2Y	4.10	0.20	0.002	77.8
Mg–4.4Zn	4.44	<0.001		112.9
Mg–1.6Zn–3.0Y	1.60	3.02	0.1	135.0
Mg–1.9Zn–2.0Y	1.89	2.04		134.5
Mg–2.0Zn–1.7Y	2.00	1.67		179.4
Mg–5.4Zn–0.6Zr	5.35		0.57	16.5

Both RT and 150 °C tension experiments were performed in air at a strain rate of 10^{-3} s^{-1} using an Instron 8562 mechanical testing machine. Samples were either electrodischarge machined or milled into a dogbone design for mechanical testing based on the ASTM C 1161. Up to five specimens per alloy were tensile tested and the reported properties were averaged. Open-air tensile–creep experiments were performed on an Applied Test System, Incorporated load frame containing a 20:1 lever-arm ratio. The testing temperatures and stresses ranged between 100 and 200 °C, and 30 and 83 MPa, respectively. Specimen temperatures were monitored by three chromel-alumel type K thermocouples located within the specimen's reduced section to maintain a temperature control of ±2 °C. The experiments were conducted such that the specimens were soaked at the creep temperature for at least 30 min prior to applying load in order to minimize the thermal stresses. Tensile displacement was measured using an extensometer/linear variable differential transducer coupling, and all temperature–strain–time data were collected using a Labview computer data-acquisition system. After the creep strain had proceeded well into the secondary regime, either the load or temperature was changed or the creep test was discontinued. The tested specimens were cooled under load to minimize recovery of the deformed structures. Selected specimens were taken to failure.

Results and discussion

Microstructure

Backscatter electron (BSE) SEM micrographs illustrating each of the microstructures are provided in Fig. 1. It is noted that the processing technique used did not result in fully-homogeneous microstructures as some chemical segregation remained. In agreement with the Mg–Zn phase diagram [29], the alloys exhibited equiaxed grains of the hexagonal close packed structure. Precipitates, of greater density than the matrix, decorated the grain boundaries. Figure 2a illustrates that for an Mg–4.1Zn–0.2Y alloy, the lighter particles at the grain boundaries were enriched in Zr. It is noted that for this sample, a Zr concentration of 0.002 wt% was measured. The matrix grains were enriched in Mg and Zn, see Fig. 2b, however, fine nanometer size laths/platelets wfere exhibited within the equiaxed grains for the Mg–2.9Zn and Mg–4.1Zn–0.2Y alloys,

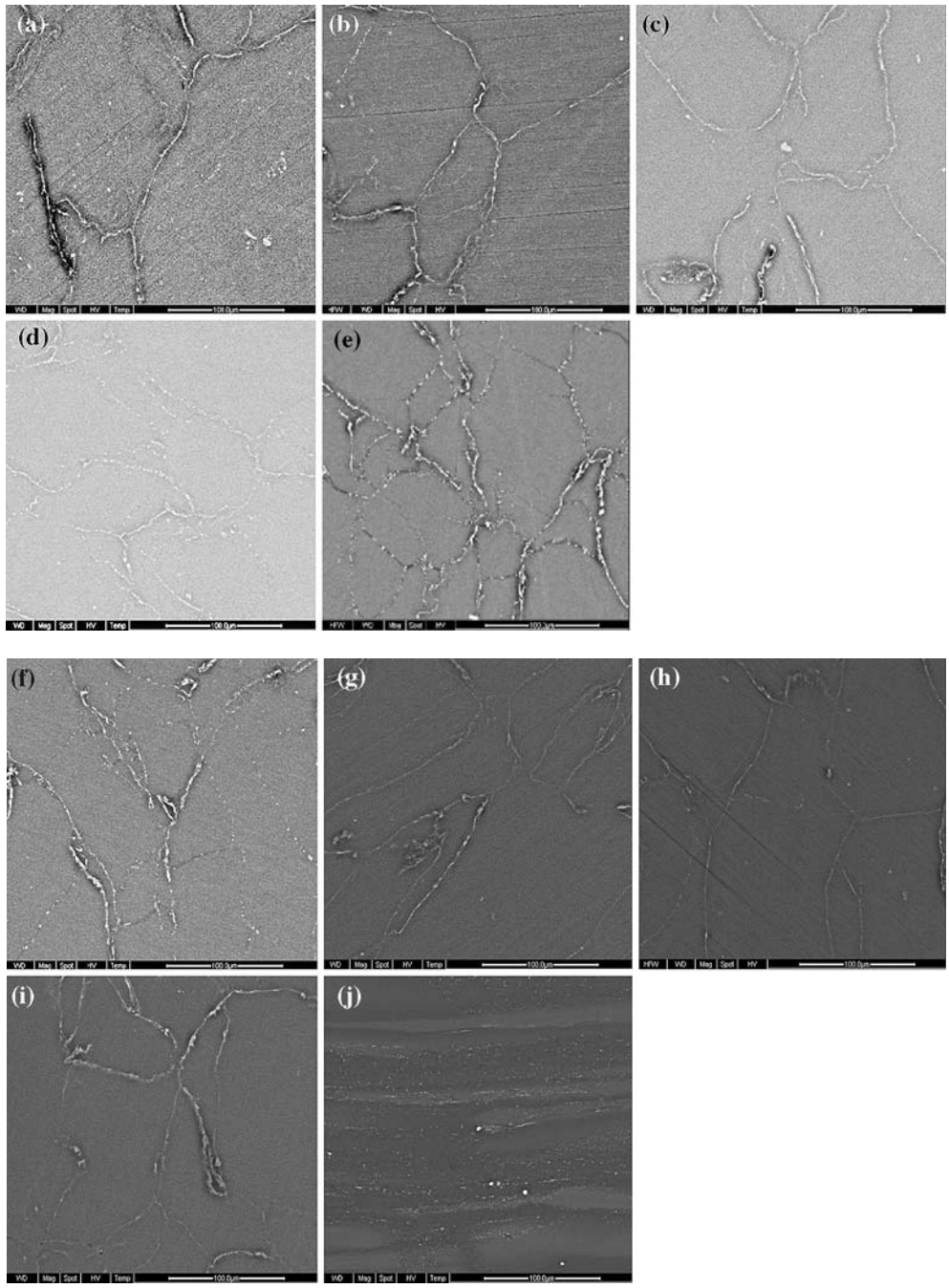

Fig. 1 BSE SEM images of the studied alloys: (**a**) 0Zn (**b**) 2.9Zn (**c**) 3.3Zn (**d**) 4.0Zn (**e**) 4.1Zn–0.2Y (**f**) 4.4Zn (**g**) 1.6Zn–3.0Y (**h**) 1.9Zn–2.0Y (**i**) 2.0Zn–1.7Y (**j**) 5.4Zn–0.6Zn

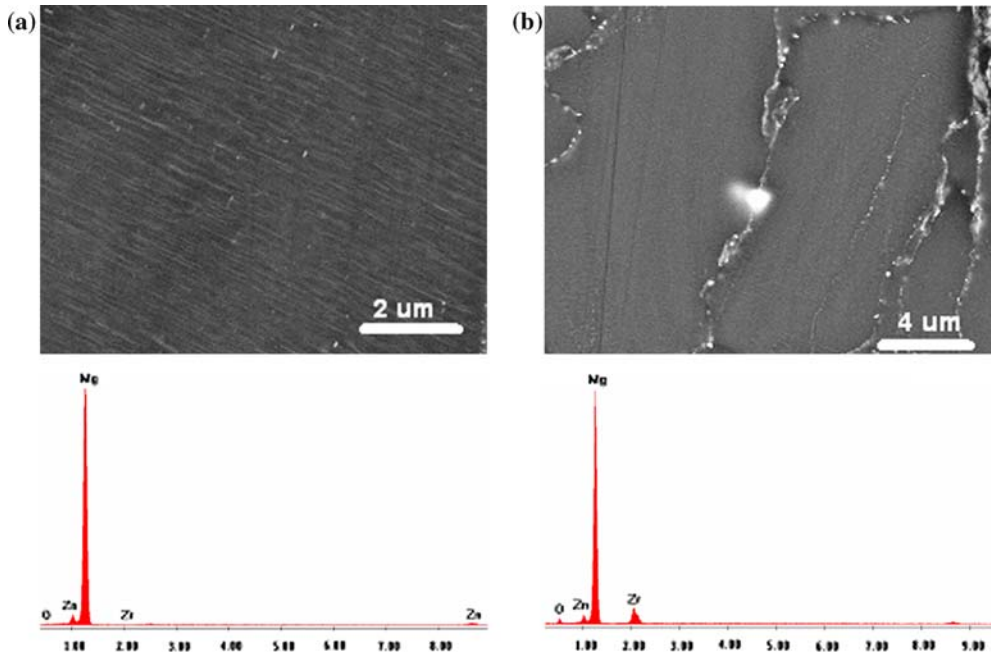

Fig. 2 SEM and EDS analysis of Mg–3.6Zn illustrating the (**a**) matrix composition enriched in Mg and Zn and (**b**) a light grain boundary particle (center) enriched in Zr, Mg, and Zn

Fig. 3a and b, where the laths' widths were finer than the resolution of the EDS technique. These laths were not observed in the other alloys. The equiaxed grain sizes of the samples varied as a function of alloy composition (Table 1). Mg–5.4Zn–0.6Zr exhibited the finest grain size and some chemical segregation was evident as depicted in Fig. 1j. One reason for the fine grain size is that Zr has proven to be a powerful grain refiner [30]. The next finest grain size was exhibited by the Mg–4.1Zn–0.2Y and Mg–4.0Zn alloys.

Properties

Tension

The RT strength values were similar for Zn concentrations between 2.9 and 4.1, where the greatest strength was exhibited by the Mg–4.1Zn–0.2Y alloy, see Table 2. The Mg–4.4Zn alloy exhibited significantly lower strength values, though its strength was greater than that for the pure Mg material. The ε_f values tended to increase with increased Zn over the entire range of Zn added, where Mg–4.4Zn exhibited a ε_f value of 8.4%. The pure Mg samples exhibited the lowest average ε_f value, 1.5%. Thus Zn increased each of the YS, UTS, and ε_f values. The Mg–1.6Zn–3.0Y, Mg–1.9Zn–2.0Y, and Mg–2.0Zn–1.7Y alloys exhibited lower UTS values than the Mg–2.9Zn alloy but similar YS and ε_f values. The strength values for the alloys with Y additions between 1.7 and 3.0 wt.% did not appear to be significantly different from each other. At 150 °C, each of the materials exhibited lower strengths than at RT, and the 150 °C ε_f values tended to be larger than those measured at RT, see Table 2.

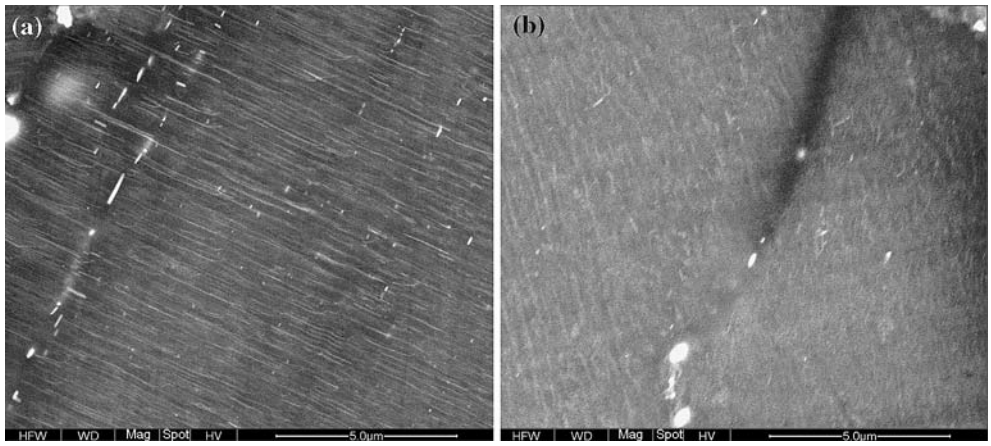

Fig. 3 Fine nanometer size laths/platelets were exhibited for (**a**) Mg–4.1Zn–0.2Y and (**b**) Mg–2.9Zn

Table 2 RT and 150 °C tensile properties

Alloy	RT			150 °C		
	0.2% YS, MPa	UTS, MPa	ε_f, %	0.2% YS, MPa	UTS, MPa	ε_f, %
Mg	61	102	1.5	50	62	1.8
Mg–2.9Zn	84	219	4.7	43	62	16.9
Mg–3.3Zn	90	210	4.6	82	93	1.6
Mg–4.0Zn	95	216	4.1	84	111	4.4
Mg–4.1Zn–0.2Y	98	223	5.0	78	116	5.4
Mg–4.4Zn	68	155	8.4	79	114	5.2
Mg–1.6Zn–3.0Y	102	150	4.1	73	109	6.9
Mg–1.9Zn–2.0Y	92	156	5.0	76	104	8.6
Mg–2.0Zn–1.7Y	83	161	5.5	66	89	4.7
Mg–5.4Zn–0.6Zr	160	283	15.0	107	130	3.9

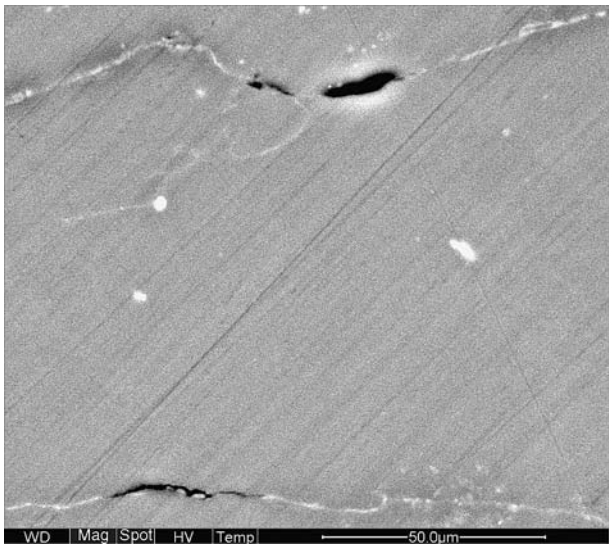

Fig. 4 SEM image of Mg after 150 °C tensile deformation (ε_f = 1.8% σ = 62 MPa). Grain boundary cracking was exhibited

The Mg–5.4Zn–0.6Zr alloy, which contained the greatest amount of Zr and a corresponding finest grain size (see Table 1), exhibited the greatest strength at RT and 150 °C. Thus small ternary additions of 0.6 wt.%Zr lead to higher strengths. For the alloys containing less than 0.1 wt.%Zr, 4.0–4.1 wt.%Zn appeared to be optimal for tensile strength both at RT and 150 °C. At 150 °C, increasing Y from 1.7 to 3.0 wt.% tended to increase the strength and ε_f values, where the Mg–2.0Zn–1.7Y alloy exhibited the lowest ε_f and strength. Thus, Y additions to Mg–Zn alloys were beneficial to the tensile strength. The Mg–4.1Zn–0.2Y alloy exhibited over 1.5 times the strength and ε_f of the pure Mg material. Thus, similar to that observed for Mg–Y alloys [13, 16], Zn is a potent strengthener for Mg and for the range of compositions examined, 4.1 wt.%Zn provided the greatest strengthening. Overall, Zn and Y alloying was beneficial to the strength and ε_f.

Deformation observations: The deformation behavior suggested that the grain boundaries were the weakest link in these alloys as after both RT and 150 °C deformation, grain boundary cracking was evident with no apparent cracking occurring within the grains, Fig. 4. Tensile fracture surfaces of the specimens depicted the ductile and brittle characteristics of the alloys and intergranular cracking as well, see Fig. 5a and b.

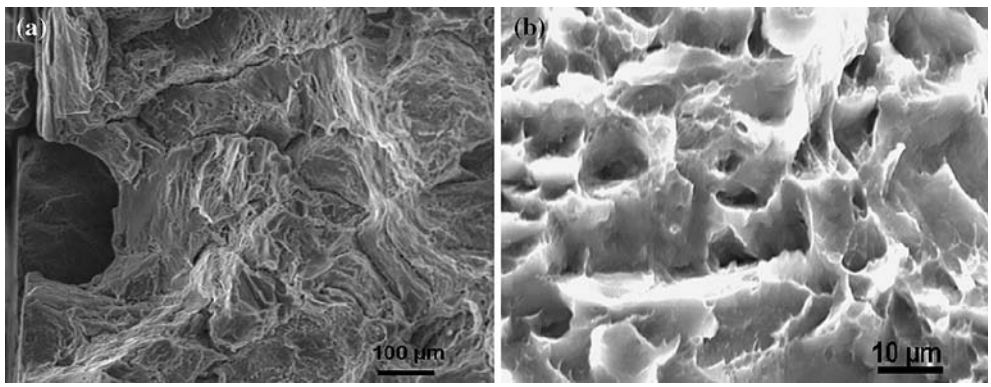

Fig. 5 SEM images of the fracture surfaces of 150 °C tensile-tested samples (**a**) Mg–1.6Zn–3.0Y which failed at 6.9% strain and exhibited intergranular cracking and (**b**) Mg–2.0Zn–1.7Y which failed at 4.7% strain and exhibited some ductile dimples

Creep

Figure 6 illustrates creep strain versus time plots for selected samples at σ = 30 MPa/T = 150 °C. It is noted that 150 °C is 0.46 the homologous temperature of Mg (assuming T_m=924 K), thus diffusional creep may be expected. No pure Mg specimens were examined in the creep study of this work. The Mg–4.1Zn–0.2Y alloy was the most creep-resistant among all the alloys tested. Thus this alloy exhibited both the greatest tensile strength and creep resistance of all the Mg–Zn and Mg-Zn-Y alloys. However, the Mg–5.4Zn–0.6Zr alloy, which exhibited the greatest tensile strength of all the alloys examined, exhibited the poorest creep resistance, Figs. 6 and 7. Comparing the creep behavior for this alloy with ''low creep'' Mg alloys containing rare earth and/or alkaline earth elements, such as AE42, AC52 (now termed AX52), AC53 (now termed AX53), and AC62 (now termed AX62), under identical applied stress and temperature conditions, Mg–5.4Zn–0.6Zr exhibited a minimum creep more than four orders of magnitude greater [11]. Mg–4.1Zn–0.2Y exhibited minimum creep rates approximately 1.5 orders of magnitude lower than those for Mg–5.4Zn–0.6Zr. Therefore, Mg–5.4Zn–0.6Zr has shown promise for ambient temperature structural applications, however, its elevated-temperature creep resistance remains a concern. The addition of Y did not improve the creep resistance as Mg–Zn–Y alloys exhibited poorer creep resistance than the Mg–Zn alloys. This is shown in Fig. 6 as the Mg–2.9Zn curve exhibited significantly lower strains than the Mg–1.6Zn–3.0Y and Mg–2.0Zn–1.7Y alloys. A closer examination of the data suggests that the addition of 4.1%Zn improves the creep resistance, and the combination of 1.7–3%Y additions provide no significant additional creep strength for Mg-1.6-2.0Zn alloys, see Fig. 8.

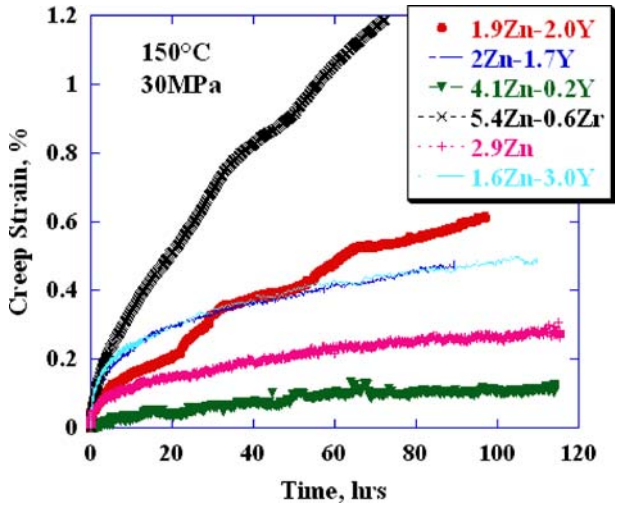

Fig. 6 Creep strain versus time plots for selected alloys at 30 MPa and 150 °C

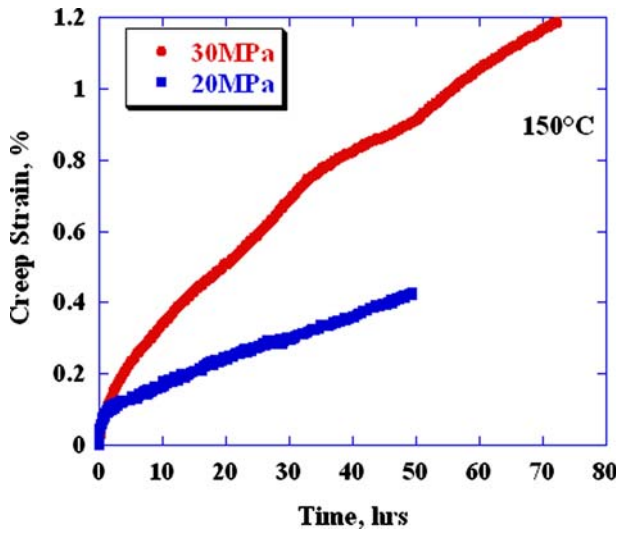

Fig. 7 Creep Strain versus time plot for a Mg–5.4Zn–0.6Zr alloy at σ = 20 MPa and σ = 30 MPa and T = 150 °C

The creep parameters were determined using the following creep law equation:

$$\dot{\varepsilon}_{\min} = B\sigma^n \exp\left(-Q_{app}/RT\right) \quad (1)$$

where $\dot{\varepsilon}_{\min}$ is the minimum creep rate B is a material-related constant, σ is the applied stress, R is the gas constant, Q_{app} is the apparent activation energy and n is the creep stress exponent. Based on this equation, the slope of the log $\dot{\varepsilon}_{\min}$ versus log σ plot at a given

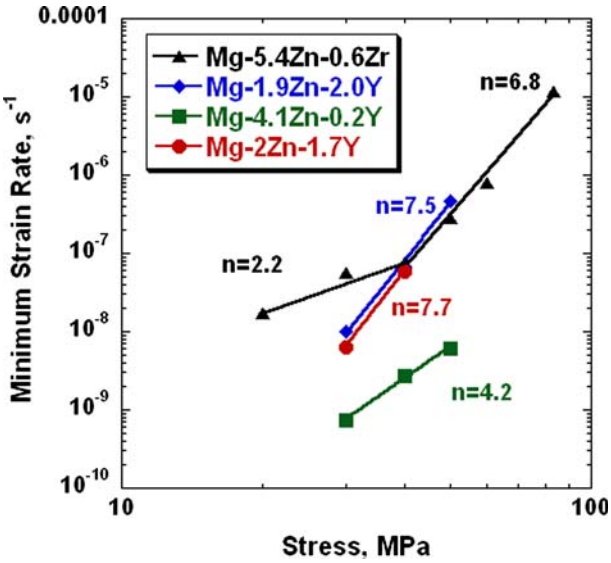

Fig. 8 Log minimum strain rate versus log stress for selected Mg alloys at 150 °C

temperature provides the stress exponent, and an Arrhenius plot (ln $\dot{\varepsilon}_{min}$ versus $1/T$) at a specific stress level will yield the Q_{app} value. The creep parameter data suggested that at least two separate creep mechanisms exist. Figures 8 and 9 illustrate plots of the stress and temperature dependence on $\dot{\varepsilon}_{min}$. At the lowest applied stress levels, $20 < \sigma < 40$ MPa, n was 2.2. For stresses greater than 40 MPa, the creep exponents were greater than or equal to 4, which suggests a dislocation climb mechanism is active. The smaller grain size of the Mg–5.4Zn–0.6Zr alloy may have promoted the transition of mechanisms as the Mg–Zn alloys did not exhibit this transition for stresses as low as 30 MPa, see Fig. 8.

Creep mechanisms at 150 °C: The stress dependence of the secondary creep rate of Mg–5.4Zn–0.6Zr tested at 150 °C is plotted in Figs. 8 and 9a, which shows a two-stage behavior with $n = 2.2$ for low applied stresses (20–40 MPa) and a much higher value of $n = 6.8$ at high stress levels (40–83 MPa). The stress exponent value at low stresses is close to that reported for other Mg–Al-based die casting alloys tested at low-stresses [11, 31]. The n-value of approximately two has been related to grain boundary sliding as the prominent creep mechanism in Mg–Al-based alloys and is supported by strong experimental evidence [31]. At higher stresses, the n-value of ~7 is slightly higher than $n \sim 5$ reported for die cast Mg alloys such as AZ91D and AS21 [31]; but is closer to that ($n = 7$) reported for a more creep-resistant magnesium alloy QE22 (Mg–2Ag–2Nd) [32], in which dislocation glide was proposed as the rate-controlling mechanism. In both ingot and die cast AZ91, creep mechanisms based on dislocation motion (on basal and non-basal planes) were proposed [33, 34], where the ingot exhibited a creep rate one order of magnitude lower than the die cast alloy which was proposed to be due to the larger grain size in the ingot microstructure. For Mg–Y alloys ranging in Y concentration from 0 to 5.6 wt.%, n was measured to be 6 for applied stresses between 30 and 80 MPa at 277 °C [13]. In this study, the stress exponent values indicate that at 150 °C, the alloys experience a grain-boundary-sliding-type of creep at a low applied stress (<40 MPa), and a dislocation-glide-controlled creep at high stresses (>40 MPa). It is noted that the finer grain size Mg–5.4Zn–0.6Zr alloy would be expected to have higher strain rates than the larger-grain alloys if grain boundary sliding was contributing significantly to the strain rates.

Creep mechanisms at 30 MPa: Figure 9b is an Arrhenius plot that gives the temperature dependence of the minimum creep rate of Mg–5.4Zn–0.6Zr under an applied stress of 30 MPa. Similarly, it shows a two-stage linear relationship: an activation energy of Q_{app}=66 kJ/mol for the temperature range of 100–150 °C; and Q_{app}=131 kJ/mol for temperatures of 150–200 °C. The Q_{app} value of 66 kJ/mol for low-temperature creep is in good agreement with other researchers [11, 31]. Dargusch and Dunlop [31] reported Q_{app} values between 36 and 44 kJ/mol for creep of AZ91D and AS21 and related it to the grain boundary sliding mechanism promoted by discontinuous precipitation of $Mg_{17}Al_{12}$ for which the activation energy is 30 kJ/mol [35]. For high-temperature (150–200 °C) creep of Mg–5.4Zn–0.6Zr, the activation energy value of 131 kJ/mol is close to 125 kJ/mol measured for high-temperature creep of pure Mg, and in the range of 92–135 kJ/mol reported for the activation energy for dislocation glide in basal planes in pure Mg which is also the self-diffusion activation energy in the Mg lattice [36]. In addition, Luo et al. [11] have measured $Q_{app} \sim 120$ kJ/mol for AC53 at 83 MPa and others have measured Q_{app} between 135 and 143 kJ/mol [37–39]. These results suggest that, for Mg–5.4 Zn–0.6Zr under an applied stress of 30 MPa, there are two creep mechanisms operating in parallel: grain boundary sliding for which the activation energy is 66 kJ/mol; and dislocation glide creep with a activation energy of 131 kJ/mol.

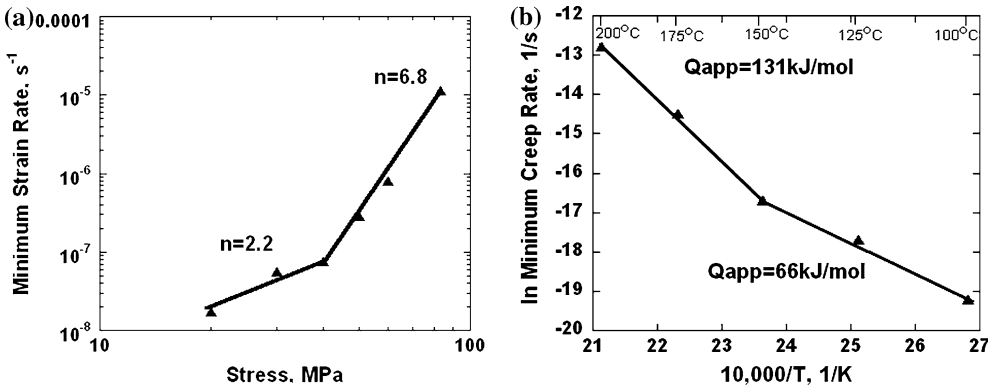

Fig. 9 (**a**) Log minimum strain rate versus log stress at $T = 150$ °C and (**b**) ln minimum creep rate versus $10000/T$ at $\sigma = 30$ MPa for a Mg–5.4Zn–0.6Zr alloy

At low temperatures (<150 °C), grain boundary sliding with a lower activation energy is suggested to dominate; and at high temperatures (>150 °C), the dislocation glide creep is suggested to dominate.

In 377 °C/30 MPa crept Mg–5.6Y–0.04Zn (Mg–1.6mol%Y–0.0015mol%Zn), bowed out dislocations were observed to trail straight dislocation segments parallel to the trace of basal planes [13]. The bowed-out dislocations were moving on prismatic planes. The dislocation densities were higher compared to those for Mg–4Y alloys with no Zn, probably due to the presence of the trailed dislocation segments. The higher dislocation density is true in the other Zn-containing alloys studies [13], where the dislocation densities were twice as high as those of the alloys without Zn. The high dislocation density is one of the origins of the improved creep resistance of the Zn-containing alloys. In addition, TEM has revealed that the activation of the non-basal slip systems is enhanced and dynamic precipitation occurred during creep deformation for Mg–Y alloys containing between 0–8 wt.% Y at 277 °C/50–200 MPa [13, 14]. The high creep resistance was correlated with two creep mechanisms: forest dislocation hardening (work hardening) and dynamic precipitation of fine pseudo-equilibrium β' phase on the dislocation lines during creep [14].

Suzuki et al. [18] suggested that the stacking fault energy in the Mg–Zn matrix decreased by the simultaneous addition of Zn and Y, whereby many planar faults are formed on (0001) matrix plane and *a*-dislocations were extended on basal planes [18]. The separation width of these extended dislocations significantly increased during creep because of the stabilization of the separation due to the segregation of Zn and Y. The separation width was also significantly affected by the interaction between opposite partial dislocation parts of extended dislocations on different but adjacent slip planes. The large separation suppresses the cross-slip and climb of dislocations, as well as the basal slip. Therefore the strengthening effects of Zn are considered to be due to the decrease in stacking fault energy and consequent reduction of mobility of dislocations. Thus the observations in this work support previous observations regarding the existence of a dislocation-controlled creep regime where Zn significantly increases the creep resistance.

Creep deformation behavior: The deformation behavior suggested that the grain boundaries were the weakest link in these alloys as grain boundary cracking was evident with no apparent cracking occurring within the grains, Figs. 10 and 11. Thus grain boundary sliding may have been accommodated by grain boundary cracking. Interestingly, the most creep resistant alloy did not exhibit grain boundary cracks, Fig. 12. Therefore greater than 0.25% creep strain was necessary to form grain boundary cracking even after 236 h of creep at 150 °C. Overall grain size and grain boundaries appear to be an important factor for the low-stress creep behavior of Mg–Zn–Zr alloys. Creep fracture surfaces of the specimens depicted the ductile and brittle characteristics of the alloys, see Fig. 13a and b.

Conclusions

1. The RT and 150 °C tensile strength of the Mg–5.4Zn–0.6Zr alloy was the greatest while Mg–4.1Zn–0.2Y was superior to all the Mg–Zn and Mg-Zn-Y alloys investigated. At 150 °C, increasing Y from 1.7 to 3.0 wt.% tended to increase the strength and ε_f values, where the Mg–2.0Zn–1.7Y alloy exhibited the lowest ε_f and strength values.
2. Tensile creep properties (total creep extension and secondary creep rate) of Mg–4.1Zn–0.2Y were significantly better than those of the other Mg–Zn and Mg-Zn-Y alloy compositions evaluated. The

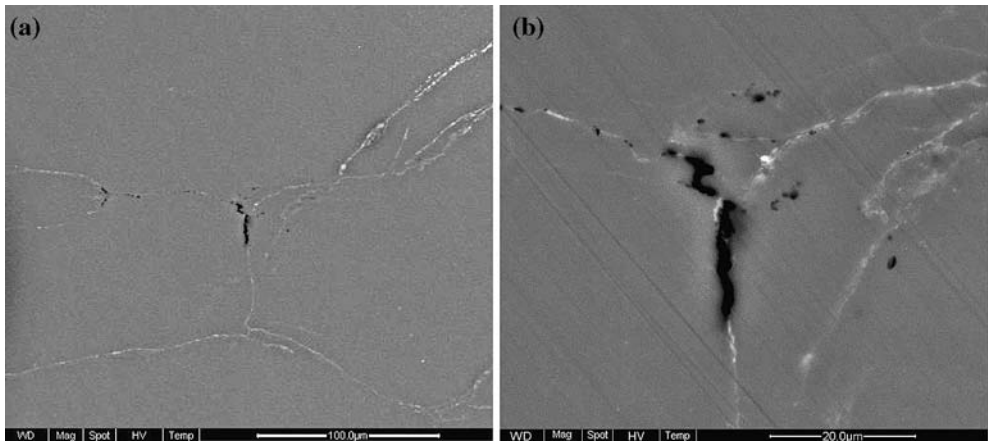

Fig. 10 (**a**) Low- and (**b**) high-magnification SEM images of a Mg–1.6Zn–3.0Y alloy after creep deformation between 30 and 50 MPa at 150 °C to ε = 2.5% for 117 h. Voids formed and coalesced at grain boundaries

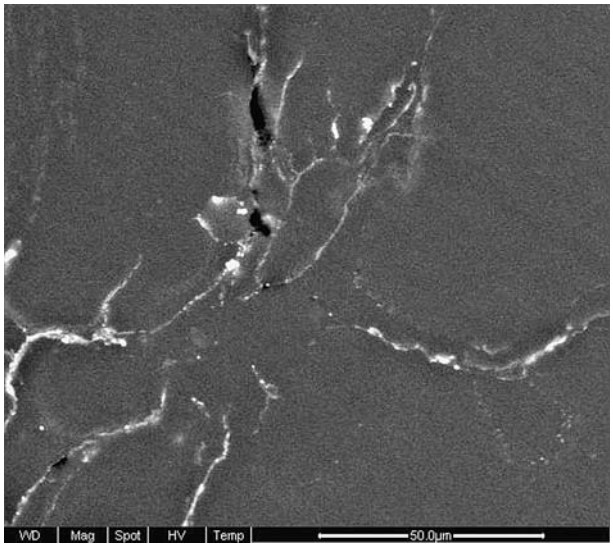

Fig. 11 BSE SEM image of a Mg–1.9Zn–2.0Y alloy after creep deformation between 30 and 50 MPa at 150 °C to $\varepsilon = 4\%$ for 133 h. Voids formed and coalesced at grain boundaries

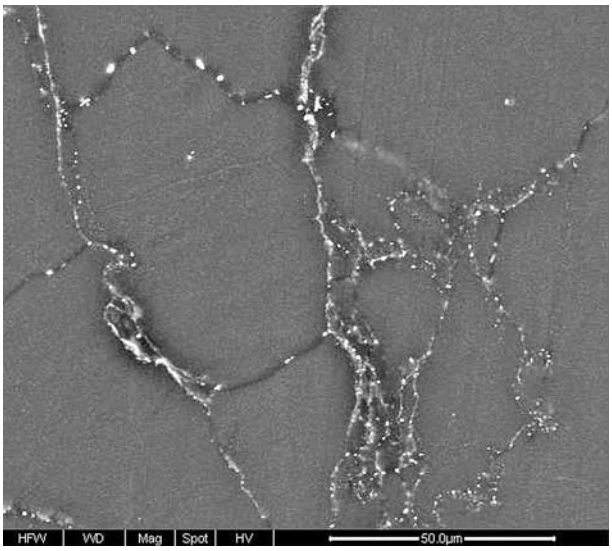

Fig. 12 SEM image of a Mg–4.1Zn–0.2Y alloy after creep deformation between 30 and 50 MPa at 150 °C to $\varepsilon = 0.25\%$ for 236 h. No grain boundary cracking was exhibited

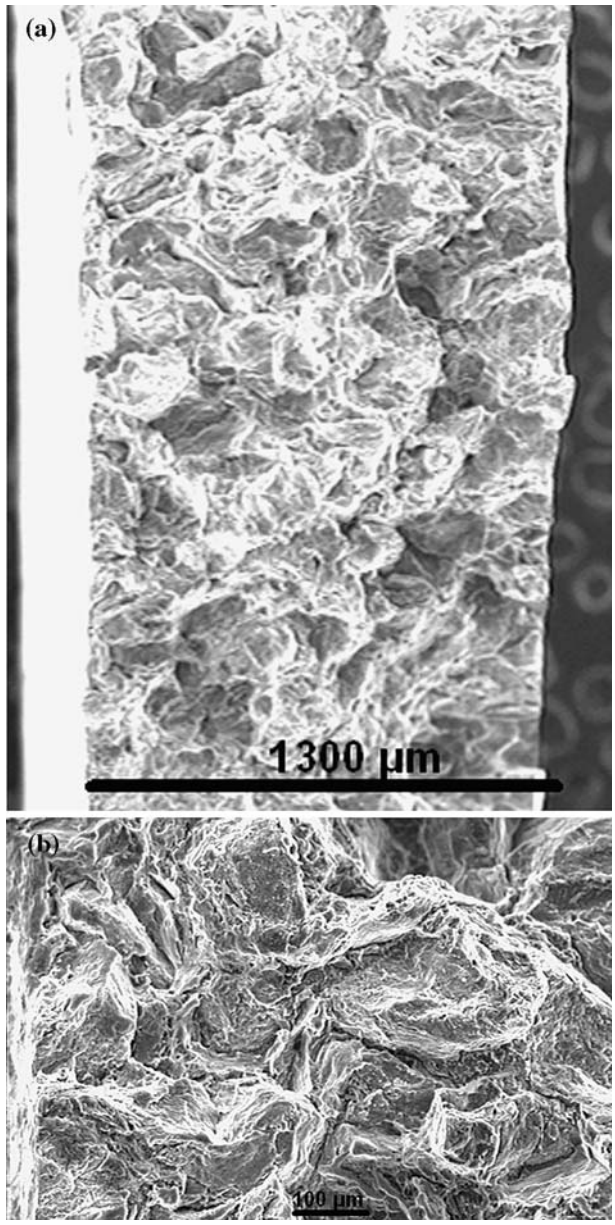

Fig. 13 (**a**) Low- and (**b**) high-magnification SEM images of the creep fracture surface of a Mg–1.9Zn–2.0Y alloy which failed after 4% strain at 150 °C after undergoing a stress jump experiment from 30 to 50 MPa for 133 h

ternary addition of Y between 1.7 and 3 wt% did not significantly affect the tensile–creep properties.

3. The stress dependency of the secondary creep rate at 150 °C suggests that the alloys experience a grain-boundary-sliding-type of creep at low applied stresses (<40 MPa), and a dislocation-controlled creep at higher stresses (>40 MPa).
4. The temperature dependency of the secondary creep rate of Mg–5.4Zn–0.6Zr at 30 MPa suggests that grain boundary sliding with a lower activation energy ($Q_{app} = 66$ kJ/mol) is in control at low temperatures (≤150 °C); while the self-diffusion ($Q_{app} = 131$ kJ/mol)-based dislocation creep takes control at high temperatures (≥150 °C).
5. The deformation behavior suggested that the grain boundaries were the weakest link in these alloys as after both RT and 150 °C deformation, grain boundary cracking was evident with no apparent cracking occurring within the grains. Overall grain

size and grain boundaries appear to be an important factor for the tensile and low-stress creep behavior of Mg–Zn alloys containing ternary Zr and Y additions.

Acknowledgements This work was partially supported by the National Science Foundation through grant DMR-0320992. The authors are grateful to Dr. Christopher Cowen and Messieurs Ken Knittel Daniel Burnett III, Matthew Dispenza and John Rich for their technical assistance.

References

1. Zhu SM, Gao X, Nie JF (2004) Mater Sci Eng A384:270
2. Moreno IP, Nandy TK, Jones JW, Allison JE, Pollock TM (2003) Scripta Mater 48:1029
3. Baril E, Labelle P, Pekguleryuz MO (November 2003) J Metals:34
4. Ozturk K, Zhong Y, Luo AA, Liu Z-K (November 2003) J Metals:40
5. Rokhlin LL (2003) Magnesium alloys containing rare earth metals structure and properties. Taylor and Francis, New York, p 211
6. Moreno IP, Sohn KY, Jones JW, Allison JE (2001) Society of Automotive Engineers paper #2001-01-0425
7. Sklenicka V, Pahutova M, Kucharova K, Svoboda M, Langdon TG (2002) Metall Trans 33A:883
8. Luo AA, Powell BR (2001) In: Hryn JH (ed) Magnesium technology. The Materials Society, Warrendale, PA, pp 137–144
9. Powell BR, Luo AA, Rezhets V, Bammarito JJ, Tiwari BL (2001) Society of Automotive Engineers paper #2001-01-0422
10. Powell BR, Rezhets V, Balogh M, Waldo R (2001) In: Hryn JH (ed) Magnesium technology. The Materials Society, Warrendale, PA, pp 175–182
11. Luo AA, MP Balogh, Powell BR (2001) Society of Automotive Engineers paper #2001-01-0423
12. Luo AA, Shinoda T (1998) Society of Automotive Engineers paper #980086
13. Maruyama K, Suzuki M, Sato H (2002) Metall Mater Trans 33A:875
14. Suzuki M, Kimura T, Maruyama K, Oikawa H (1998) Mater Sci Eng A252:248
15. Suzuki M, Inoue R, Sugihara M, Sato H, Koike J, Maruyama K, Oikawa H (2000) Mater Sci Forum 350–351:151
16. Suzuki M, Kimura T, Koike J, Maruyama K (2003) Mater Sci Forum 426–432:593
17. Suzuki M, Kimura T, Koike J, Maruyama K (2003) Scripta Mater 48:997
18. Suzuki M, Kimura T, Koike J, Maruyama K (2004) Mater Sci Eng A387–389:706
19. Sato T (1999) Mat B Jpn Inst Metals 38:294
20. Kawamura Y, Hayashi K, Inoue A, Masumoto T, (2001) Mater Trans 42:1172
21. Inoue A, Kawamura Y, Matsushita M, Hayashi K, Koike J (2001) J Mater Res 16:1894
22. Inoue A, Matsushita M, Kawamura Y, Amiya K, Hayashi K, Koike J (2002) Mater Trans 43:580
23. Abe E, Kawamura Y, Hayashi K, Inoue A (2002) Acta Mater 50:3845
24. Ping DH, Hono K, Kawamura Y, and Inoue A (2002) Phil Mag Lett 82:543
25. Nishida M, Kawamura Y, Yamamuro T (2004) Mater Sci Eng A375–377:1217
26. Watanabe H, Mukai T, Ishikawa K, Mabuchi M, Higashi K (2001) Mater Sci Eng A307:119
27. Watanabe H, Mukai T, Higashi K (1988) Superplastic forming. The Minerals, Metals, and Materials Society, Warrendale, PA, p 179
28. Standard Test Methods for Determining Grain Size Designation E 112–88 (1988) American Society for Testing and Materials (ASTM), West Conshohocken, PA, pp 228–253
29. ASM Handbook (1992) Alloys and phase diagrams (vol 3). ASM International, Materials Park, OH, p 285
30. Emley EF (1966) Principles of magnesium technology, 1st edn. Pergamon Press, Oxford, New York
31. Dargusch MS, Dunlopm GL (1998) In: Mordike BL, Kainer KU (ed) Magnesium alloys and their applications. Werkstoff-Informationsgesellschaft, Frankfurt, Germany, pp 277–282
32. Mordike RL, Lukac P (1997) Proceedings of the 3rd International Magnesium Conference. The Institute of Metals, London, England, pp 419–429
33. Regev M, Aghion E, Rosen A, Bamberger M (1998) Mater Sci Eng A252:6
34. Regev M, Aghion E, Rosen A (1997) Mater Sci Eng A234–236:123
35. Uchida H, Shinya T (1995), J Jpn Inst Light Metals 45(10): 572
36. Dieter GE (1986) Mechanical metallurgy. McGraw-Hall, New York, NY, pp 432
37. Vagarali SS, Langdon TG (1982) Acta Metall 30:1157
38. Blum W, Watzinger B, Weidinger P (1998) In: Mordike BL, Kainer KU (eds) Magnesium alloys and their applications. Werkstoff-Informationsgessellschaft mbH, Frankfurt, Germany, pp 49–60
39. Watzinger B, Weidinger P, Breutinger F, Blum W, Rosch R, Lipowsky H, Haldenwanger H-G (1998) In: Mordike BL, Kainer KU (eds) Magnesium alloys and their applications. Werkstoff-Informationsgessellschaft mbH, Frankfurt, Germany, pp 259–264